Fatigue Property of Additively Manufactured Ti-6Al-4V under Non-proportional Multiaxial Loading

Yuya Kimura
Ritsumeikan University: Ritsumeikan Daigaku
Fumio Ogawa
Tohoku University: Tohoku Daigaku
Takamoto Itoh (itohtaka@fc.ritsumei.ac.jp)
Ritsumeikan University: Ritsumeikan Daigaku https://orcid.org/0000-0002-3210-3982

Original Article

Keywords: Additive manufacturing , Ti-6Al-4V , Low cycle fatigue , Multiaxial stress , Non-proportional loading , Internal defect

DOI: https://doi.org/10.21203/rs.3.rs-139256/v1

Abstract

Low cycle fatigue strength properties of additively manufactured Ti-6Al-4V alloy were experimentally investigated under proportional and non-proportional multiaxial loading. Fatigue tests have been conducted by means of hollow cylinder specimens with and without heat treatments, at room temperature in air. Fatigue tests with proportional loading represented by a push-pull strain path and non-proportional loading represented by a circle strain path were conducted, respectively. The fatigue lives of additively manufactured specimens were drastically reduced obviously by internal voids and defects in comparison with the specimens used in the previous study [1]. In addition, the defect size is measured, and the defect does not cause fatigue strength reduction above some size. The fracture surface was observed using SEM to investigate fracture mechanism of additively manufactured specimens under two types of strain path. Different fracture patterns are recognized for the two strain paths; however, both showed the retention of the crack propagation in spite of the presence of numerous defects. The crack propagation properties of the materials with numerous defects under non-proportional multiaxial loading were elucidated to increase the reliability of additive manufactured components.

1 Introduction

Additive manufacturing (AM) has enabled to fabricate complex geometry parts, to lighten weight, and to shorten processing time due to the creation of subsequent thin cross-sections of a component and represents one of the most innovative fabrication technologies in recent years [2–4]. However, AM has a lot of process parameters, and the process control is extremely difficult. Moreover, the defects and residual stresses are arisen by thermal expansion or thermal contraction in a manufacturing process [2–8]. Therefore, AM mostly is not recognized practicable because strength reliability of AM parts is inferior to traditional manufacturing technologies such as casting, forging and rolling in general [9–10]. Accordingly, to widen the applicability of AM parts, fatigue strength properties of additively manufactured components need to be accurately understood.

The titanium alloy Ti-6Al-4V is currently employed, mostly in the aeronautical and medical fields, because it has the properties of high strength, excellent thermal and corrosion resistance and biocompatibility. On the other hand, material cost is expensive, and the machinability is worse. From the above, Ti-6Al-4V is considered to be a good material for AM [11]. Uniaxial high cycle fatigue tests for AM Ti-6Al-4V have been widely analyzed; however the research on low cycle fatigue strength under non-proportional multiaxial loading in which principal direction of stress or strain changes in a cycle has not yet been reported [12–18].

In this study, low cycle fatigue tests under non-proportional multiaxial loading were conducted by means of additively manufactured specimen. In addition, the fracture mechanism of AM components with defects was investigated by the fracture surface observation. Then, the factor of the decrease in fatigue strength was discussed focusing on internal defects, that have hardly been clarified in the previous study [1].

2 Laser Powder Bed Fusion

The laser powder bed fusion (L-PBF) is the most employed technique for fabrication of additively manufactured components. The steps of the fabrication technique are represented schematically in Figure 1 [19], and manufacturing processes are shown below: 1. Layer of powdered material is applied to building platform; 2. Powdered material is solidified into a cross-section of a 3D model with laser; 3. Building platform is lowered. The next layer of powder is applied; 4. The process repeats itself until the creation of the part is complete; 5. The part is removed from the unused powder.

As the advantages, L-PBF can economically fabricate ideal parts with complex geometries in a rapid design to manufacturing cycle. However, as the disadvantages, the components fabricated by L-PBF have voids, residual stresses and surface roughness due to the influence of different process parameters. For the improvement, performing HIP and sandpapering can remove voids and surface roughness, respectively. Thus, fatigue strength of AM components can be improved.

3 Low Cycle Fatigue Tests

3.1 Testing Machine

Figure 2 and Figure 3 show a schematic view and a photo of the electrical servo-controlled tension torsion fatigue testing machine. The testing machine is equipped with 2 types of cylinders for axial and torsion loading, and it enables to generate non-proportional loading. The maximum axial load is 50 kN, and maximum torque is 500 Nm. The load cell was equipped for load measurement, and the extensometer which has equipped the eddy current sensor was employed to detect axial strain and shear strain, simultaneously. Figure 4 shows a schematic view of the extensometer attached onto the specimen.

3.2 Material and Specimen

The material tested was titanium alloy Ti-6Al-4V. Figure 5 show the shape and dimensions with no machining process and the resultant hollow cylinder specimen which has a 9 mm inner diameter, an 11 mm outer diameter, and 12 mm parallel part. The types of specimens were with (HT) and without (NHT) heat treatment to remove the residual stresses. The layer was laminated perpendicular to the longitudinal direction of the specimen. The specimens were polished with an alumina powder solution (particle size 1 μm) on the external surface and with a sand paper with #2000 grit on the internal surface to avoid the influence of surface roughness on fatigue life. A parallel part of the specimens has numerous defects; However, the number of defects differs for each of them.

3.3 Test Condition

The testing machine that can perform tensile and torsion tests was used to apply both proportional and non-proportional loading paths to the specimens. The proportional loading path is represented by push-

pull strain path (PP), whereas the non-proportional loading path is represented by circle strain path (CI) in which axial and shear strain have 90 degrees-out-of-phase. In the CI, the intensity of the von Mises' equivalent strain was constant while the direction of the principal strain changes during the cycle. The axial and shear strain were measured using an extensometer with a 12 mm strain gage length connected to the specimens. The applied strains are visualized in Figure 6. The test temperature was room temperature in air, and strain rate $\dot{\varepsilon}_{eq}$ = 0.2 %/s was applied. Fatigue tests were conducted under strain control. Number of cycles to failure (failure life) was defined when axial and shear stress amplitude decreased to 3/4 of the maximum stress recorded.

4 Experimental Results And Discussion

4.1 Fatigue Properties

Figure 7 shows the test results correlated the von Mises' equivalent strain amplitude $\Delta\varepsilon_{eq}/2$ with the failure life N_f. Figure 8 shows the generated hysteresis loops for $0.5N_f$ and the maximum stress behavior during the tests in each test condition.

The results (Fig. 7) of fatigue tests under PP clearly show that the data scatter is not so drastic and were within the factor of 3 bands. Moreover, they were no difference between heat treatment and no heat treatment. It is considered the temperature for heat treatment was not sufficient to remove residual stresses. However, the data of PP HT ($\Delta\varepsilon_{eq}$ = 1.3 %) exhibited lower failure lives and out of the factor of 3 bands. In Fig. 8 (a), (b) and (e), the hysteresis loops and the maximum stress amplitude at $\Delta\varepsilon_{eq}$ = 1.3 % were compared. The hysteresis loops indicated the almost same elastic deformation. The maximum stress amplitude for NHT remains almost constants. Then probably, the crack initiated from the vicinity of N_f, and the failure occurred very quickly after the crack initiation. On the other hand, for HT, the maximum stress amplitude decreased instantly from around $0.3N_f$. Therefore, the crack was considered to initiate from $0.3N_f$, and after some crack propagation, the failure took place.

Failure life (Fig. 7) under CI was reduced compared to PP resulting in 10% decrease in fatigue life. The scattering of data was also very small; however, it cannot be confirmed due to limited data (the presence of the only one data of CI NHT ($\Delta\varepsilon_{eq}$ = 0.5%)), the reduction in failure life for NHT cannot be seen. For the other material such as stainless steel and carbon steel, in case of low strain level, the failure life is the almost same as PP, but it is not clear for this study due to limited data. In Fig. 8 (c), (d) and (f), the hysteresis loops and the maximum stress amplitude of $\Delta\varepsilon_{eq}$ = 0.5% were compared. In case of low strain level, the hysteresis loops also exhibited the almost same elastic deformation. The maximum stress amplitude for two data was similar in deformation behavior. Although the overload was seen in the data of HT, it is estimated that there is almost no effect because it could be adjusted in 10 cycles. Therefore, why this data shows the longer life than other data remains as question. The previous test results are also shown in Fig. 7 [1]. In the previous study data, failure lives were longer than that of this study. The specimens of the previous study were the same material (Ti-6Al-4V) but were fabricated with a different

manufacturing condition. Based on the above-mentioned, the internal defects were investigated to quantify the size of defects.

4.2 Internal Defects

Figure 9 compares the internal defects between the previous study and this study. In the previous study, the small defects were observed inside, but in this study, the internal defects depend on the observation site. AM components have usually the defects inside, and fatigue strength of the material depends on size and density of the defect; however, the defects size does not affect the fatigue life above a certain size because the results of fatigue tests (Fig. 7) shows a clear correlation regardless of various defect size. It is necessary to investigate the dependence of fatigue strength reduction on defect size.

4.3 Fracture Surface

Figure 10 shows the pictures of fracture surface after fatigue tests, and the observation surface is perpendicular to the specimen axis. It is difficult for main crack initiation site to be analyzed as for specimens of this study. The cracks were initiated from the boundary of partly melted defects regardless of strain range and strain paths, and the stress concentration in the defects causes premature rupture in comparison to the results which were obtained with the same material [1]. From Figure 10 (a2) and (b2), the crack propagation patterns were divided into the first phase (from the crack initiation site to the crack middle site) and the second phase (form the crack middle site to the crack end site) during test. In the first phase of the test, the propagation path was different due to strain paths, and it is possible that high stress existed evidenced by rougher fatigue fracture surfaces. In PP, the crack propagated simply, but in the CI, it became complicated. Basically, due to the change of the principal direction of stress and strain during the cycle in CI, maximum shear stress plane is changed in the cycle. Thus, there is a possibility for the crack to initiate and propagate to many directions. In the second phase of the test, fatigue fracture surfaces were with the similar pattern, and the crack propagation seems to be suppressed. It is estimated that a local non-propagating effect under multiaxial stress took place. Thus, it is possible that the change of the crack propagation pattern in each phase of the test is a characteristic of AM components with numerous defects, and it is noticeable under non-proportional multiaxial loading.

From this study, the fatigue strength is absolutely inferior to that of the previous study and traditionally manufactured components; however, there is a possibility that AM technology is used for the mechanical structure because the non-propagating effect of cracks was verified under non-proportional multiaxial loading.

Conclusions

(1) The failure lives under PP and CI were almost not affected by heat treatment performed to remove residual stresses due to insufficient temperature. In PP, the data scatter is not so drastic and almost all data were within the factor of 3 bands. In CI, although the scattering of data was also very small, failure life under CI was reduced compared with PP resulting in 10% decrease in failure life.

(2) The small defects were observed inside in previous study, and the defects were larger in this study. Stress concentration at the boundary of defects was generated, and the results of fatigue test shows a clear correlation, so the size of defects above a certain size does not affect the failure life.

(3) Regardless of strain range and strain paths, the cracks were initiated from the boundary of partially melted defects, indicating that stress concentration in the defect caused premature rupture compared to the results obtained with the same material.

(4) In the first phase of the test, the propagation path was different due to strain paths; however, in the second phase of the test, fatigue fracture surfaces were with the similar pattern, and the crack propagation seems to be suppressed.

Declarations

Acknowledgements

We would like to thank TRUMPS SISMA SRL for providing the material for the test specimen.

Funding

Supported by JSPS KAKENHI Grant Number 18H05256.

Availability of data and materials

The datasets supporting the conclusions of this article are included within the article.

Authors’ contributions

The author’ contributions are as follows: Yuya Kimura was in charge of performing fatigue tests and writing manuscript; Fumio Ogawa observed fracture surfaces; Takamoto Itoh directed this study.

Competing interests

The authors declare no competing financial interests.

Consent for publication

Not applicable

Ethics approval and consent to participate

Not applicable

References

1. S Bressan, F Ogawa, T Itoh, F Berto. Cyclic plastic behavior of additively manufactured Ti-6Al-4V under uniaxial and multiaxial non-proportional loading. *International Journal of Fatigue*, 2019, 126: 155-164.
2. J P Kruth, M C Leu, T Nakagawa. Progress in additive manufacturing and rapid prototyping. *CIRP Annals*, 1998, 47: 525-540.
3. GN Levy, R Schindel, J P Kruth. Rapid manufacturing and rapid tooling with laser manufacturing (LM) technologies, state of the art and future perspectives. *CIRP Annals*, 2003, 52: 589-609.
4. J Deckers, J Vleugels, J P Kruth. Additive Manufacturing of Ceramics. *Journal of Ceramics Science and Technology*, 2014, 5: 245-260.
5. P Mercelis, J Kruth. Residual stresses in selective laser sintering and selective laser melting. *Rapic Prototype Journal*, 2006, 12: 254-265.
6. M Shiomi, K Osakada, K Nakamura, T Yamashita, F Abe. Residual stress within metallic model made by selective laser melting process. *CIRP Annals*, 2004, 53: 195-198.
7. S Leuders, M Thöne, A Riemer, T Niendorf, T Tröster, HA Richard, et al. On the mechanical behaviour of titanium alloy TiAl6V4 manufactured by selective lasermelting: fatigue resistance and crack growth performance. *International Journal of Fatigue*, 2013, 48: 300-307.
8. B Baufeld, E Brandl, O van der Biest. Wire based additive layer manufacturing: comparison of microstructure and mechanical properties of Ti-6Al-4V components fabricated by laser-beam deposition and shaped metal deposition. *Journal of Materials Processing Technology*, 2011, 211: 1146-1158.
9. A Fatemi, R Molaei, S Sharifimehr, N Shamsaei, N Phan. Torsional fatigue behavior of wrought and additive manufactured Ti-6Al-4V by powder bed fusion including surface finish effect. *International Journal of Fatigue*, 2017, 100: 347-366.
10. A Fatemi, R Molaei, S Sharifimehr, N Phan, N Shamsaei. Multiaxial fatigue behavior of wrought and additive manufactured Ti-6Al-4V by powder bed fusion including surface finish effect. *International Journal of Fatigue*, 2017, 99: 187-201.
11. T Nakano. Additive manufacturing for titanium and its alloys. *The Japan Institute of Light Metals*, 2017, 67: 470-480.
12. P Li, DH Warner, A Fatemi, N Phan. Critical assessment of the fatigue performance of additively manufactured Ti–6Al–4V and perspective for future research. *International Journal of Fatigue*, 2016, 85: 130-143.

13. A Sterling, N Shamsaei, B Torries, SM Thompson. Fatigue behaviour of additively manufactured Ti-6Al-4V. *Procedia Engineering*, 2015, 133: 576-589.
14. K Kanazawa, KJ Miller, MW Brown. Cyclic deformation of 1% Cr-Mo-V steel under out-of-phase loads. *Fatigue & Fracture of Engineering Materials & Structurest*, 1979, 2: 217-228.
15. E Krempl, H Lu. Comparison of the stress responses of an aluminum alloy tube to proportional and alternate axial and shear strain paths at room temperature. *Mechanics of Materials*, 1983, 2: 183-192.
16. T Itoh, M Sakane, M Ohnami, K Ameyama. Effect of stacking fault energy on cyclic constitutive relation under nonproportional loading. *Journal of the Society of Materials Science, Japan*, 1992, 41: 1361-1367.
17. T Itoh, T Yang. Material dependence of multiaxial low cycle fatigue lives under nonproportional *International Journal of Fatigue*, 2011, 33: 1025-1031.
18. M Wu, T Itoh, Y Shimizu, H Nakamura, M Takanashi. Low cycle fatigue life of Ti-6Al-4V alloy under non-proportional loading. *International Journal of Fatigue*, 2012, 44: 14-20.
19. T Nakano, T Ishimoto. Powder-based Additive Manufacturing for Development of Tailor-made Inplants for orthopedic Applications. *KONA Powder and Particle Journal*, 2015, 32: 75-84.

Figures

Figure 3

Photo picture of fatigue testing machine

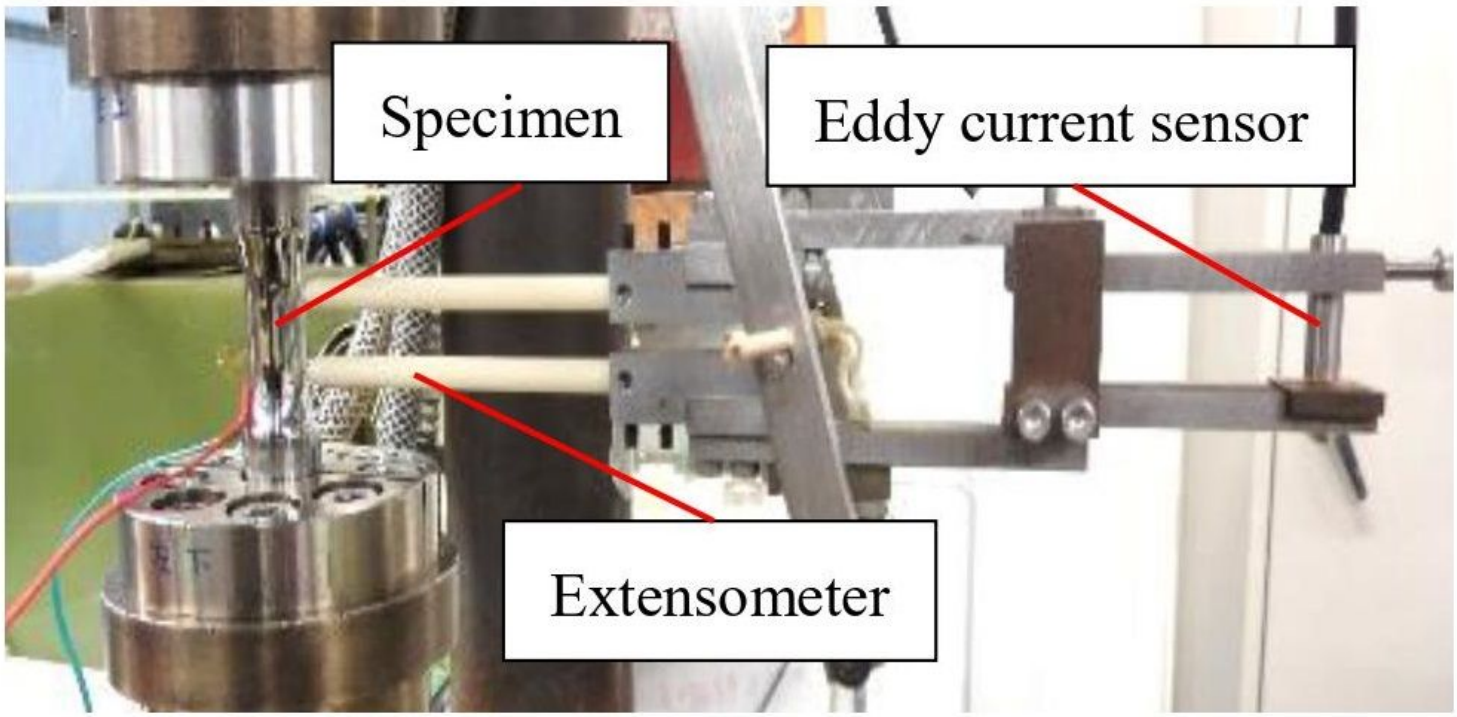

Figure 4

State of lever type extensometer during fatigue test

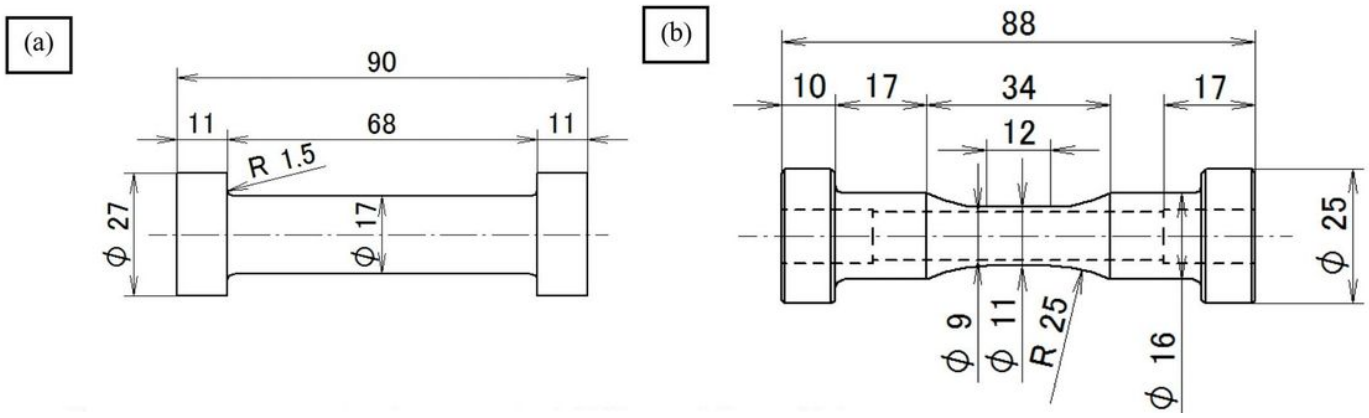

Figure 5

Shape and dimensions of specimen after (a) L-PBF and (b) the machining process

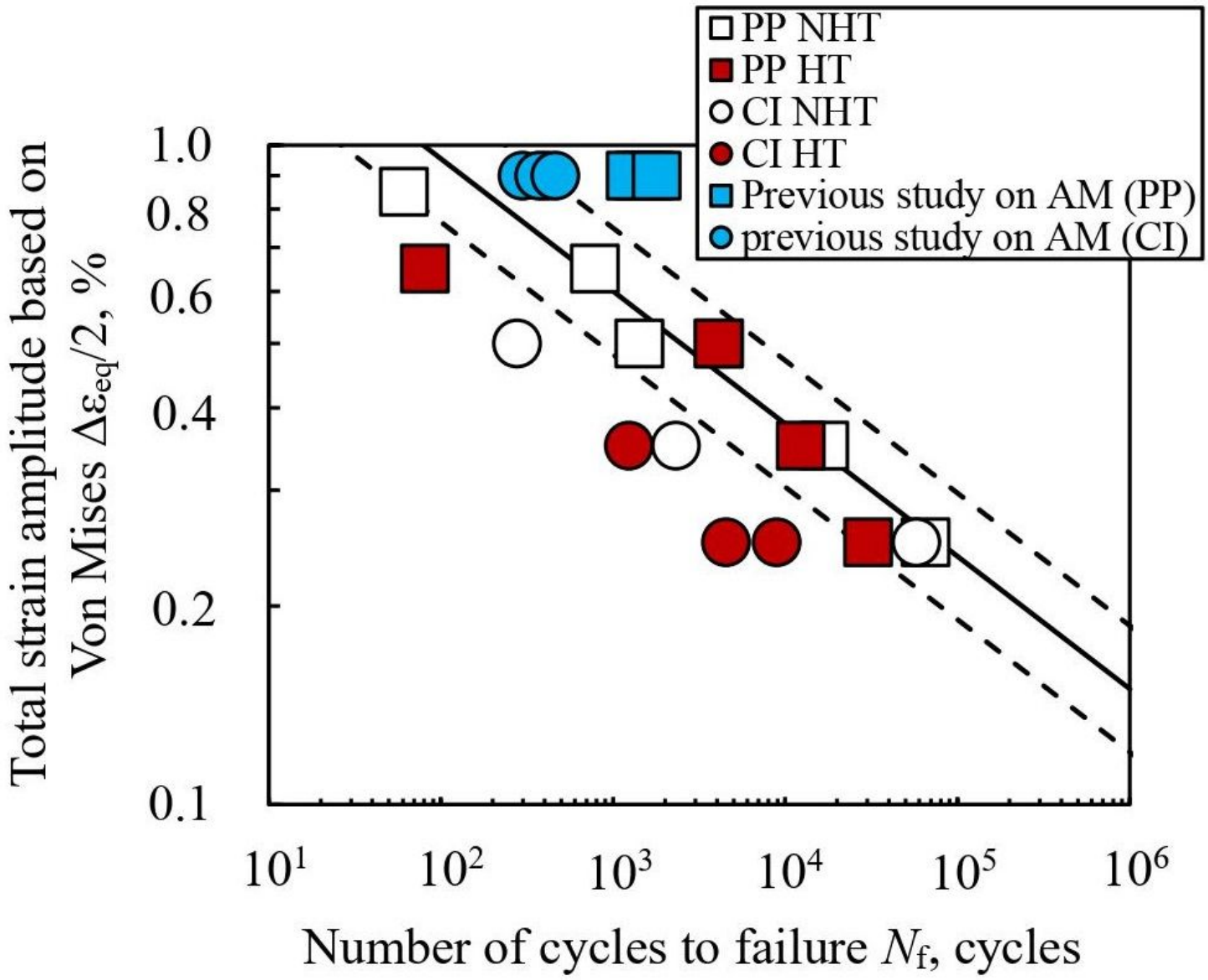

Figure 7

Relationship between Mises equivalent strain amplitude Δεeq/2 and failure life Nf

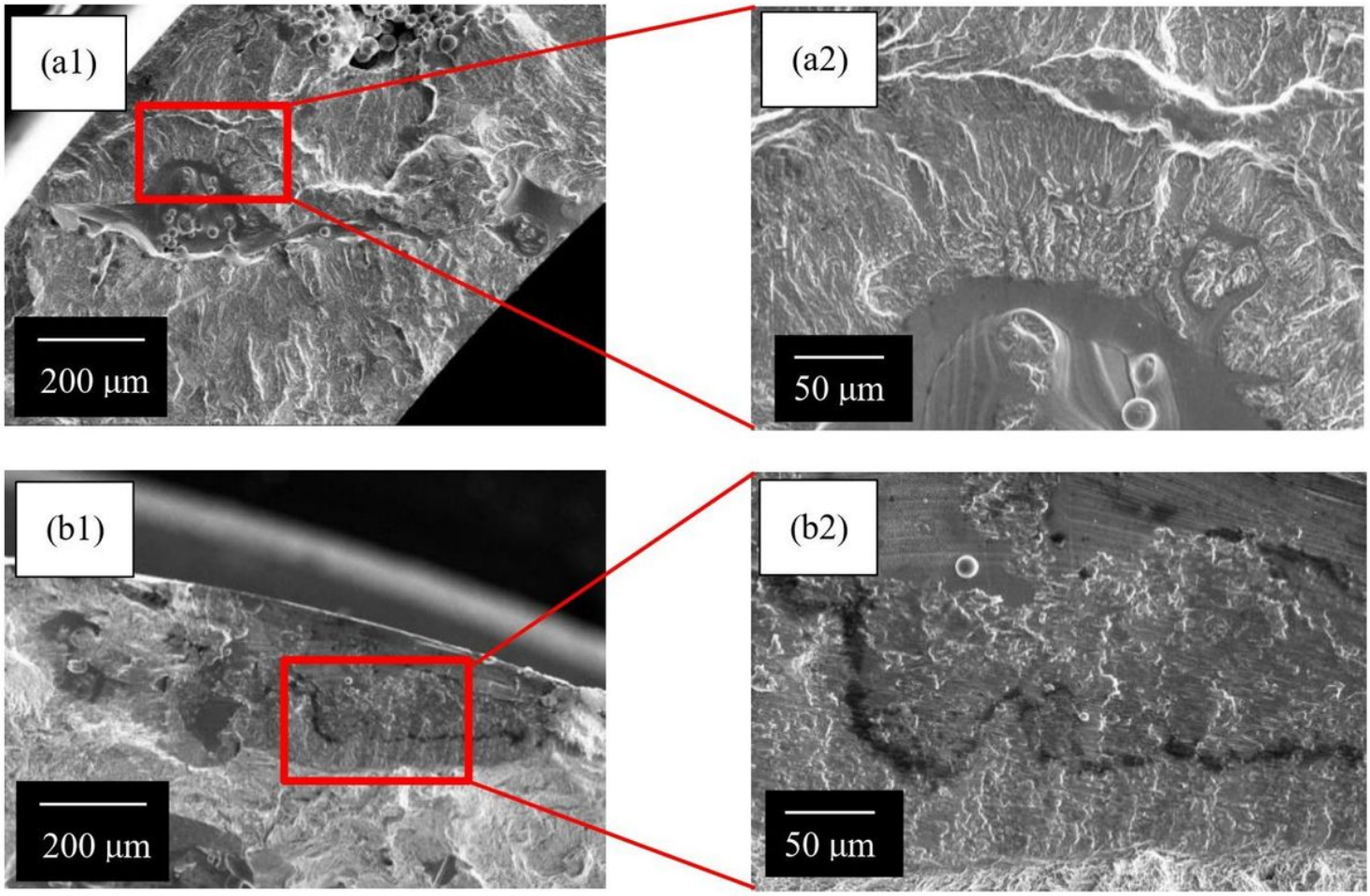

Figure 10

SEM images of the fracture surface; (a) push-pull strain path and (b) circle strain path